2009 American Control Conference
Hyatt Regency Riverfront, St. Louis, MO, USA
June 10-12, 2009

Optimal Design and Observation of Counter-Current Autothermal Reactors for the Production of Hydrogen

Michael Baldea and Monica Zanfir and Prodromos Daoutidis

Abstract— **Autothermal reactors, coupling endothermic and exothermic reactions in parallel channels, represent one of the most promising technologies for hydrogen production. Building our our prior results, the present work focuses on hydrogen generation in counter-current autothermal reactors. Using a first-principles model, we demonstrate that simply reversing the flow in a reactor designed for co-current operation leads to the formation of hot spots and a decrease in thermal efficiency. Thus, we propose a redesign strategy based on establishing the optimal length of the catalytic surface for both the reforming and the combustion channels, with the objective of minimizing the difference between the channel temperatures. We demonstrate that the redesigned reactor exhibits superior steady state performance and improved dynamic operability. Finally, in view of facilitating model-based controller design, we introduce a reduced-order model based observer for the counter-current autothermal reactor and validate its operation via a simulation study.**

I. Introduction

The interest in economically efficient hydrogen production has been steadily increasing, and even more so recently, given the progress made in the development and implementation of fuel cell technologies. Autothermal reactors, combining exothermic and endothermic reactions are one of the most promising hydrogen production technologies, featuring in-situ heat generation, which allows for increased fuel efficiency and a compact size[1]. From a design and operation point of view, autothermal reactors rely either on a constant, unidirectional flow, whereby the raw material for hydrogen production and the necessary fuel flow in different, parallel channels of the reactor (either in co-current or counter-current), or on flow reversal, in which case the catalyst bed within the reactor acts as a heat trap [2].

The majority of the research studies concerning the design and operation of autotermal reactors of either category investigate the steady-state behavior of the system. However, in the context of integrating such reactors in larger systems that include fuel cells for power production, the transient operation of the autothermal reactor, enabling variable levels of hydrogen supply in response to varying power requirements to a fuel cell downstream becomes much more interesting [3]. Thus, the availability of accurate, reliable and, at the same time, computationally efficient models is of great importance for dynamic analysis and control [4]. Due to the inherent multiple-time scale behavior of autothermal reactors [5], their dynamic models are ill conditioned and challenging to simulate, and recent efforts have been aimed at providing an approach for deriving models of reduced dimensions that capture the salient dynamic features of the original system [6].

In our previous work [7], we have considered the dynamic behavior of co-current autothermal reactors. Using arguments from singular perturbation theory, we documented the existence of two distinct time scales in their dynamic behavior, indicating the physical parameters that are at the origin of this feature. Via an asymptotic analysis, we derived reduced-order, nonlinear models for the dynamics in each time scale. In particular, we showed that the derived slow model corresponds to generally accepted empirically derived simplified models for the class of reactors considered.

Subsequently, we presented illustrative dynamic simulation results using the rigorous model of a hydrogen production reactor, identifying the issues posed by the transient operation of such reactors, and demonstrating that they are alleviated by the implementation of feedback control.

Motivated by the low energy efficiency of co-current autothermal reactors (due to the elevated feed and effluent temperatures required in their operation), in the present paper we focus on hydrogen generation in counter-current autothermal reactors. Using a first-principles reactor model [7] we initially demonstrate that a simple flow reversal in a reactor designed for co-current operation leads to the formation of an exit hot spot, detrimental to the efficiency of the reactor. Thus, we propose a redesign strategy based on establishing the optimal length of the catalytic surface for both the reforming and the combustion channels, with the objective of minimizing difference between the channel temperatures. We demonstrate that the redesigned reactor exhibits superior steady state performance and improved dynamic operability. Finally, in view of facilitating model-based controller design, we introduce a reduced-order model based observer for the counter-current autothermal reactor and validate its operation via a simulation study.

II. System description

We consider the case of an autothermal reactor for generating hydrogen from methane and steam via methane/steam reforming (MSR)

$$\begin{aligned} CH_4 + H_2O &\rightarrow H_2 + CO, \quad \Delta H_{298} = +206 kJ/mol \\ CH_4 + 2H_2O &\rightarrow H_2 + CO_2, \quad \Delta H_{298} = +165 kJ/mol \end{aligned} \tag{1}$$

and water-gas shift (WGS):

$$CO + H_2 \rightarrow CO_2 + H_2, \quad \Delta H_{298} = -41 kJ/mol \tag{2}$$

M.B. and M.Z. are at Praxair Technology Center, Tonawanda, NY 14150. P.D. is with the Department of Chemical Engineering and Materials Science, University of Minnesota, Minneapolis MN 55455, USA. Please direct correspondence to: michael_baldea@praxair.com (Michael Baldea)

978-1-4244-4524-0/09/$25.00 ©2009 AACC

The steam reforming reactions are endothermic and require a significant source of heat. We assume that a monolithic tubular reactor is used, and that the MSR/WGS reactions only occur in half of the monolith channels. The remaining channels are dedicated to providing the heat required by the endothermic MSR/WGS reactions via the catalytic combustion of methane– MCC– (fed as a mixture of methane and air).

$$CH_4 + 2O_2 \rightarrow CO_2 + H_20, \quad \Delta H_{298} = -802.6kJ/mol \tag{3}$$

The case of the co-current operation of the reactor (*i.e.,* the flow in the exothermic and endothermic channels occurs in the same direction is illustrated in Figure **??**.

We assume that the chemical reactions occur only at the catalytic surface and no homogenous reactions are taken into account. Also, we consider that the reaction rates account for the diffusion of the reactants and products to/from the surface (*i.e.,* diffusion to the surface is not modeled explicitly) and write material balance equations only for the gas phase. Furthermore, without loss of generality, we analyze only two parallel channels of the reactor (this analysis can be easily extended to more channels or to the entire reactor). Under these assumptions, the operation of the reactor is modeled by a system of coupled, partial differential equations for the material and energy balances for the reaction channels and the solid surface:

$$\rho_{g,k}\frac{\partial w_{j,k}}{\partial t} = -\bar{V}_k\rho_{g,k}\frac{\partial w_{j,k}}{\partial z} + D_{\text{eff},k}\rho_g\frac{\partial^2 w_{j,k}}{\partial z^2} + \sum_{i=1}^{n}\nu_{j,i}M_j a_v r_i(\underline{w}_k, T_{g,k}) \tag{4}$$

$$\rho_{g,k}C_{pg,k}\frac{\partial T_{g,k}}{\partial t} = -\bar{V}_k\rho_{g,k}C_{pg,k}\frac{\partial T_{g,k}}{\partial z} + \lambda_{\text{eff},k}\frac{\partial^2 T_{g,k}}{\partial z^2} + \alpha_k a_v(T_{g,k} - T_s) \tag{5}$$

$$\rho_s C_{ps}\frac{\partial T_s}{\partial t} = \lambda_s\frac{\partial^2 T_s}{\partial z^2} - \sum_{k=1,2}\alpha_k a_v(T_{g,k} - T_s) - \sum_{k=1,2}\sum_{i=1}^{n} a_v r(\underline{w}, T_{g,k})\Delta H_i \tag{6}$$

where w_j represents the mass fraction of component j, T represents the temperature, C_p is the constant pressure heat capacity, ρ the density, λ, the thermal conductivity, α the heat transfer coefficient, D_{eff} the effective diffusion coefficient, M_j the molecular mass of component j, a_v the area/volume ratio of the solid catalyst, r_i the reaction rate of reaction i, $\nu_{i,j}$ the stoichiometric coefficient of component j in reaction i. The index g denotes the gas phase, (with $k \in 1, 2$ denoting the channel of the said gas phase), while the index s refers to the solid.

The nominal parameters of the reactor are presented in Table I:

The physical properties of the gas in the endothermic side were assumed to be close to those of steam, while the gas in the exothermic side was assumed to have physical properties similar to air. The reader is referred to [7] for the more details.

TABLE I
BASE CASE REACTOR CONDITIONS

Length, m	0.5	
Channel height, m	0.026	
Gas phase	Steam Reforming Side	Combustion Side
Feed Temperature	793 K	600 K
Feed Pressure	1.5 bar	3 bar
Inlet velocity	0.6 m/s	5 m/s
$w_{CH_4,inlet}$	0.2499	0.02
$w_{O_2,inlet}$	0	0.218
$w_{H_2O,inlet}$	0.7500	0
$w_{H_2,inlet}$	0.0001	0

For the endothermic side, material balance equations are written for menthane, water, hydrogen, carbon monoxide and carbon dioxide, and for the exothermic channels, for oxygen and methane, making for a total of 10 coupled partial differential equations (PDEs). The partial differential equation system was then solved using the method of lines. Equations 4, 5 and 6 were discretized in the spatial domain using a finite difference approximation. The first derivatives were approximated with forward finite differences, while second derivatives were approximated with centered finite differences for numerical stability. The space domain was discretized using 90 equidistant nodes, resulting in an ODE system with 900 degrees of freedom. It was verified through simulations that an increase in the number of nodes did not lead to significant improvements in the accuracy of the solution.

We used Dirichlet boundary conditions at the feed point for the material and energy balances in the gas phase, and Neumann boundary conditions for the material and energy balance equations at the reactor exit, as well as for the energy balance on the catalyst wall at $z = 0$ and $z = L$. The boundary conditions were also implemented using the finite difference approach.

The discretized system was implemented in Matlab and the stiff solver `ode15s` was used to obtain the transient numerical solution.

III. STEADY STATE ANALYSIS

Co-current autothermal hydrogen generation via steam-methane reforming requires that the reactants be fed at a high temperature (in excess of 600K), which, in turn, entails the use of a preheater and, consequently, an additional energy expenditure, to operate the reactor. Elevated effluent temperatures (Figure 1) are an additional source of energy inefficiency. On the other hand, counter current reactor designs (whereby the fuel and reforming feed points are located at the opposite ends of the reactor) accept lower temperature feed streams and operate at lower outlet temperatures (thereby ensuring that less energy leaves the system with the effluents).

Autothermal methane-steam reforming operating in counter-current with the supporting exothermic reaction thus

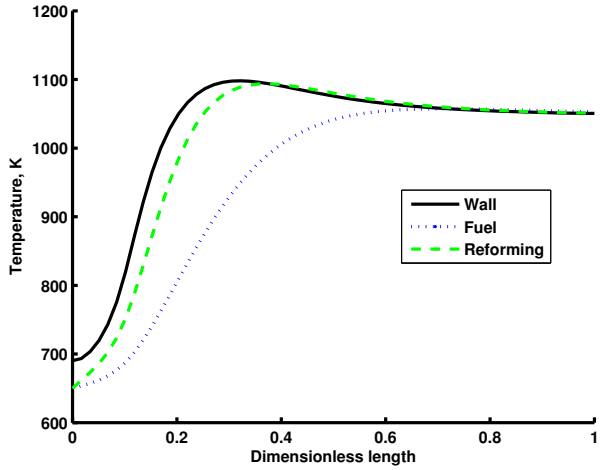

Fig. 1. Longitudinal temperature profile of the co-current reactor

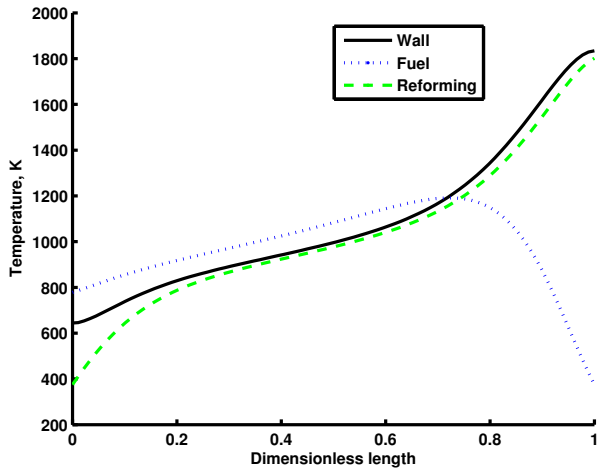

Fig. 2. Longitudinal temperature profile of the counter-current reactor

In this case, the temperature of the reforming channel exhibits a profile that increases longitudinally from the feed point to the reactor exit. This temperature rise is due to the elevated rate of heat generation at $z = L$, the spatial coordinate that corresponds to the the exit of the reforming channel as well as to the inlet of the combustion channel. A fast reaction, combustion proceeds rapidly at $z = L$, leading to a significant temperature rise in the reforming channel.

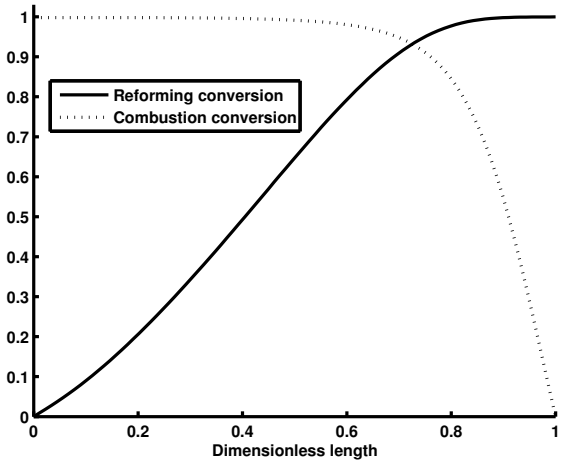

Fig. 3. Longitudinal conversion profile of the counter-current reactor

represents an interesting alternative to co-current operation. Using a previously developed first-principles reactor model [7], we initially studied the effect of reversing the flow direction in the combustion channel. The reactor parameters were maintained at the values listed in Table I, with the exception of imposing lower feed stream temperatures (375K for the combustion side and 400K for the reforming side). The steady-state longitudinal temperature profiles in the reforming and combustion channels, as well as the wall temperature along the reactor are presented in figure 2.

The desired reforming conversion (Figure 3) is thus obtained at the cost of operating the reactor at an unacceptably high temperature. Consequently, the need for a reactor redesign

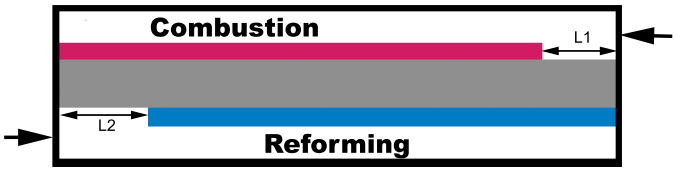

Fig. 4. Decision variables in the optimal redesign of the counter-current reactor

IV. Optimal Redesign of the Counter-Current Reactor

We approach the redesign of the counter-current autothermal reactor by identifying an optimal catalyst distribution in the combustion and reforming channels. A stepwise catalyst distribution is considered in both channels, such that a portion of length L_i, $i = 1, 2$ near the channel inlet is catalyst free (Figure 4) and acts as a heat exchanger. Thus, in solving the optimization problem, we seek L_1 and L_2 that minimize the maximum temperature difference between the channels along the reactor. Specifically, we aim to solve the optimization problem:

$$\begin{aligned} \min_{L_1,L_2} \quad & \| T_{comb} - T_{ref} \|_\infty \\ s.t. \quad & steady\ state \\ & \eta_{1,2} > 0.9 \\ & L_1 < L,\ L_2 < L \end{aligned} \tag{7}$$

with η_1 and η_2 denoting, respectively, the conversion in the combustion and reforming channels.

Owing to the reduced number of decision variables, it was possible to address the solution of the problem (8) via the

exhaustive exploration of the parameter space (Figure 5), leading to the optimal values $L_1 = 0.3\ L$ and $L_2 = 0$, with L being the total reactor length. The temperature profile that results from using the optimal catalyst distribution is presented in Figure 6. Comparing this profile with that of the original reactor (Figure 2), we note that the steady-state operation of the optimized reactor features significantly lower feed and exit temperatures and, implicitly, a higher energy efficiency due to lowering the energy expended in preheating the feed streams and reducing energy losses via the effluent streams.

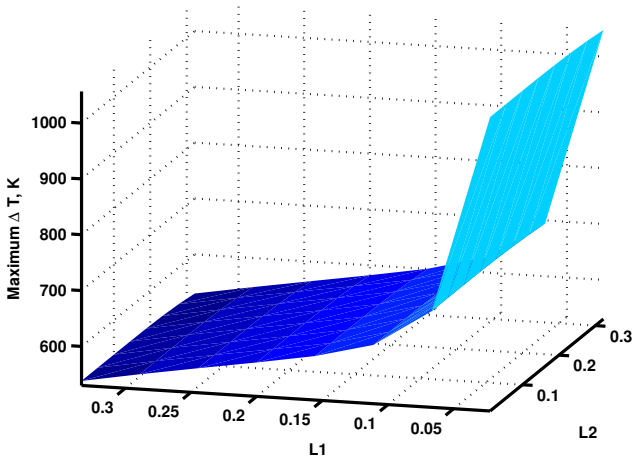

Fig. 5. Maximum $\Delta T = |T_1 - T_2|$ as a function of catalyst free length

Remark 1: Figure 5 presents the variation of the maximum temperature difference as a function of the catalyst distribution. Note that the distribution of the reforming catalyst does not influence significantly the maximum temperature difference. On the other hand, the maximum temperature difference is strongly dependent on the catalyst distribution in the combustion channel. These results are consistent with the findings presented in Section III: relocating the beginning of the catalytic portion of the combustion channel away from the channel entrance allows the fuel mixture to be preheated, and, more importantly, transfers the zone characterized by intense heat generation (i.e., the initial length of combustion catalyst) towards the feed point of the reforming mixture. The latter feature allows the reforming mixture to reach the temperature required by the activation energy of the reactions over a short reactor length, with sufficient channel length remaining for the mixture to reach the desired conversion without exceeding any operating temperature limits.

Remark 2: Note that the formulation (8) of the optimization problem employs the ∞-norm (corresponding to minimizing the *maximum* of the temperature difference between the reforming and combustion channels along the reactor length) rather than the 2-norm (in which case the solution of the optimization problem would consist of finding the values of the decision variables that result in the minimum *average* temperature difference). The proposed formulation

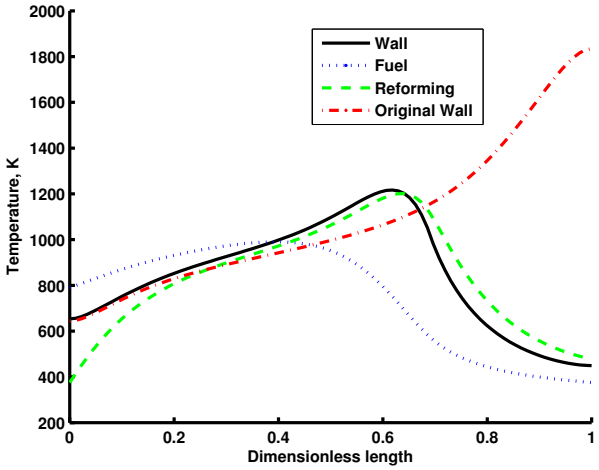

Fig. 6. Temperature profile in the counter-current reactor with optimal catalyst distribution

presents the benefit of precluding the formation of sharp temperature peaks caused by a large mismatch between the rate of heat generation by combustion and the rate at which heat is absorbed by the endothermic reactions.

V. Dynamic Analysis

In the context of integrating an autothermal reactor for hydrogen production in a larger energy generation system, the dynamic behavior of the reactor in response to transient requirements originating *e.g.* in a downstream fuel cell is of primary importance. In our previous work [7] we have demonstrated that co-current autothermal reactors exhibit a complex dynamic behavior. Furthermore, we have demonstrated that, absent a control system, it is possible for reaction extinction to occur in a co-current reactor under normal operating conditions. Figure 7 presents such a case, whereby reactor extinction occurs upon increasing the required hydrogen generation rate (via increasing the feed flowrate to the endothermic side) by 50%.

The design paradigm of the counter-current reactor (a high temperature "hot core" between relatively low temperature "cold ends") increases the robustness of the system to such transitions, as demonstrated in Figure 8, whereby an identical disturbance (a 50% increase in the reforming mixture flowrate) leads, as expected, to a decrease in conversion. The conversion degradation is, however, not followed by the complete extinction of the reactor.

VI. High-Gain Observer Development

The real-time solution of the discretized full-order model (Equations 4-6) for the purpose of state observation is challenging. In order to circumvent the difficulties typically associated with solving such large-scale, stiff systems, we exploited our previous results [7], along with a reduction technique for the energy balance equations [8] in order to obtain a non-stiff model of significantly reduced dimensions.

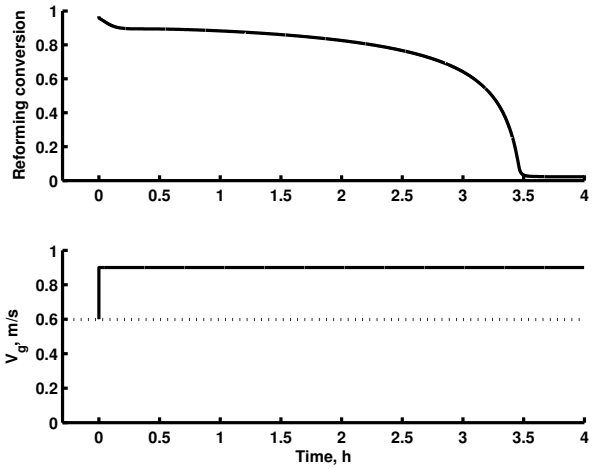

Fig. 7. Evolution of the reforming conversion of the co-current reactor in the case of a 50% increase in the reforming mixture flowrate

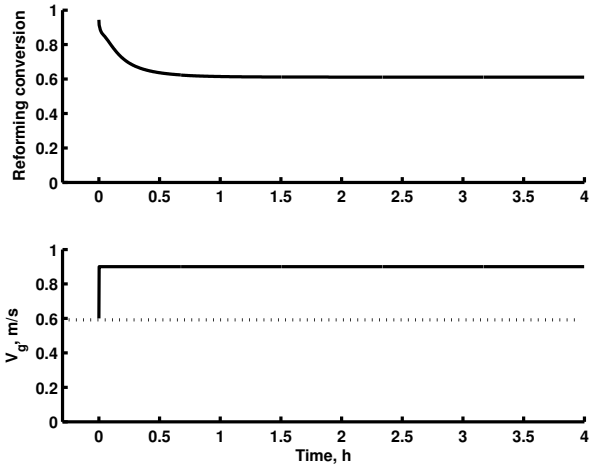

Fig. 8. Evolution of the reforming conversion of the counter-current reactor in the case of a 50% increase in the reforming mixture flowrate

In particular, in our previous work we showed that the dynamics of the fluid phase evolve in a time scale that is faster than the time scale in which the temperature of the solid evolves. In light of these facts, both the energy and material balance equations of the fluid phase were replaced by their quasi-steady state equivalents.

Furthermore, we assumed that the contribution of conduction to the energy balance of the fluid phase is negligible (an assumption that is justified by its low Péclet number). We the used a MacLaurin expansion [8] to compute the temperature of the fluid in each channel as a function of the temperature of the catalytic wall. Truncating the series after the first-order term we obtain:

$$T_{g,k} = T_s - \frac{\rho_{g,k} C_{pg,k} V_{g,k}}{\alpha_k a_v} \frac{\partial T_{g,k}}{\partial z} \tag{8}$$

The substitution of Equation 8 in the energy balance equation for the wall allows for the energy balance of the entire reactor to be captured by a single equation.

In order to further reduce the complexity of the material balance equations we resorted to the use of a coordinate transformation. The transformed coordinates employ, respectively, the reaction extent variables Ψ_1 , and Ψ_2 and Ψ_3 for the combustion, MSR and WGS reactions, rather than weight fractions, to capture the composition of the gas phase. The coordinate transformation is defined such that, for the combustion side:

$$\begin{aligned} y_{CH_4,1} &= y^0_{CH_4,1} - \Psi_1 \\ y_{O_2,1} &= y^0_{O_2,1} - 2\Psi_1 \\ y_{CO_2,1} &= \Psi_1 \\ y_{H_2O,1} &= 2\Psi_1 \end{aligned} \tag{9}$$

and for the reforming side:

$$\begin{aligned} y_{CH_4,2} &= \frac{y^0_{CH_4,2} - \Psi_2}{1 - 2\Psi_2} \\ y_{H_2O,2} &= \frac{y^0_{H_2O,2} - \Psi_2 - \Psi_3}{1 - 2\Psi_2} \\ y_{H_2,2} &= \frac{3\Psi_2 + \Psi_3}{1 - 2\Psi_2} \\ y_{CO,2} &= \frac{\Psi_2 - \Psi_3}{1 - 2\Psi_2} \\ y_{CO_2,2} &= \frac{\Psi_2}{1 - 2\Psi_2} \end{aligned} \tag{10}$$

with y_i being the mole fraction of component i and the superscript 0 being used to specify an inlet mole fraction.

Using the temperature equivalence in Equation 8 and the transformed coordinates Ψ_i, the model of the reactor becomes:

$$\begin{aligned} \rho_s C_{ps} \frac{\partial T_s}{\partial t} &= \lambda_s \frac{\partial^2 T_s}{\partial z^2} - \sum_{k=1,2} V_{g,k} \rho_{g,k} C_{pg,k} \frac{\partial T_s}{\partial z} \\ &\quad - \sum_{k=1,2} \sum_{i=1}^{n} a_v r_i(\underline{\Psi}, T_s) \Delta H_i \end{aligned} \tag{11}$$

$$\begin{aligned} 0 &= -\bar{V}_k \frac{\partial \Psi_{k,m}}{\partial z} + D_{\text{eff},k} \frac{\partial^2 \Psi_{k,m}}{\partial z^2} \\ &\quad + \bar{M}_{g,k,0} \sum_{i=1}^{n} \frac{a_v}{\rho_{g,k}} r_i(\underline{\Psi}, T_s) \end{aligned} \tag{12}$$

with $m = 1$ for the combustion channel and $m = 2, 3$ for the reforming channel. $\bar{M}_{g,k,0}$ represents the average molecular mass of the feed mixture in channel k.

The reduced order model in Equations 11-12 was discretized over a grid with 40 nodes and the method of lines was used for integration. We assumed that 5 equally spaced sensors are available in the combustion catalytic area, and two additional sensors are used: one located at the position of the reactor temperature peak (considered to be the axial location of the wall temperature peak during steady state operation at the nominal, design operating conditions), the other located at the exit of the reforming channel.

We used the discretized reduced-order model in the formulation of a high-gain sate observer. The resulting observer is thus described by a DAE system of the form:

$$\frac{dT_n}{dt} = \boldsymbol{A}(\underline{T},\underline{\Psi})\underline{T} + \underline{f}(\underline{T},\underline{\Psi}) + \boldsymbol{K}(\underline{T} - \underline{\hat{T}}) \quad (13)$$
$$0 = \boldsymbol{B}(\underline{T},\underline{\Psi})\underline{T} + \underline{\phi}(\underline{T},\underline{\Psi})$$

where the matrices $\boldsymbol{A}$ and $\boldsymbol{B}$ originate in the finite difference discretization of the spatial derivatives of the temperature and extent of reaction, and the nonlinear functions $\underline{\phi}$ and $\underline{f}$ capture, respectively, the effect of the reactions on the material balance and on the energy balance equations. $\underline{\hat{T}}$ represents the vector of measured temperatures obtained from the distributed sensors, and $\boldsymbol{K}$ is the observer gain.

We carried out a simulation study with to evaluate the performance of the observer. For the purpose of this study, the inlet velocity of the reforming mixture was varied and the response of the reactor (in terms of reforming conversion) computed by the full-order model was compared to the conversion computed by the state observer. The results are presented in Figure 9.

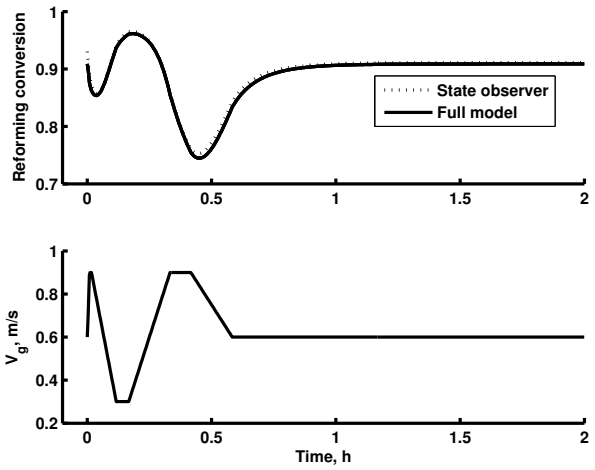

Fig. 9. Transient evolution of model and observed reforming conversion

Notice that the proposed observer exhibits a very good performance: the data obtained from the full-order model simulation and those obtained from the observer are in excellent agreement.

VII. CONCLUSIONS

In this work, we have focused on on hydrogen generation in counter-current autothermal reactors. Using a first-principles model, we initially demonstrated that a simple flow reversal in a reactor designed for co-current operation leads to the formation of hot spots and a decrease in thermal efficiency. Consequently, we developed an optimal redesign strategy based on establishing the optimal length of the catalytic surface for both the reforming and the combustion channels, with the objective of minimizing the difference between the channel temperatures. The resulting optimal design featured lower feed and effluent temperatures than its co-current counterpart, having a higher energy efficiency owing to reducing the energy expenditure in the preheater and the energy losses via hot effluent streams. We also demonstrated that the redesigned reactor exhibits an improved dynamic performance when compared to the original co-current design. Finally, in view of facilitating model-based controller design, we proposed a reduced-order model based observer design for the counter-current autothermal reactor and validated its performance with a simulation study. Our future work will rely on the proposed observer design to formulate a nonlinear, model-based control strategy for autothermal reactors. The results of this work will constitute the subject of a future publication.

REFERENCES

[1] R. Ramaswamy, P. Ramachandran, and M. Dudukovic, "Recuperative coupling of exothermic and endothermic reactions," *Chem. Eng. Sci.*, vol. 61, pp. 459–472, 2006.

[2] G. Kolios, J. Frauhammer, and G. Eigenberger, "Autothermal fixed-bed reactor concepts," *Chem. Eng. Sci.*, vol. 55, pp. 5945–5967, 2000.

[3] H. Gorgun, M. Arcak, S. Varigonda, and S. A. Bortoff, "Observer designs for fuel processing reactors in fuel cell power systems," *Int. J. Hydrogen Energ.*, vol. 30, pp. 447–457, 2005.

[4] K. M. Vanden Bussche, S. N. Neophytides, I. A. Zolotarskii, and G. F. Froment, "Modeling and simulation of the reversed flow operation of a fixed-bed reactor for methanol synthesis," *Chem. Eng. Sci.*, vol. 48, pp. 3335–3345, 1993.

[5] N. S. Kaisare, J. H. Lee, and A. G. Fedorov, "Hydrogen generation in a reverse-flow microreactor. parts I and II," *AIChE J.*, vol. 51, pp. 2254–2272, 2005.

[6] A. Gorbach, G. Eigenberger, and G. Kolios, "General approach for the reduction of detailed models for fast cycling processes," *Ind. Eng. Chem. Res.*, vol. 44, pp. 2369–2381, 2005.

[7] M. Baldea and P. Daoutidis, "Dynamics and control of autothermal reactors for the production of hydrogen," *Chem. Eng. Sci.*, vol. 62, pp. 3218–3230, 2007.

[8] V. Balakotaiah and S. Dommeti, "Effective models for packed-bed catalytic reactors," *Chem. Eng. Sci.*, vol. 54, pp. 1621–1638, 1999.